Interactions of negative strain rate sensitivity, martensite transformation, and dynamic strain aging in 3rd generation advanced high-strength steels

Michael Callahan, Astrid Perlade, Jean-Hubert Schmitt

Interactions of negative strain rate sensitivity, martensite transformation, and dynamic strain aging in 3rd generation Advanced High-Strength Steels

Michael Callahan[a,*], Astrid Perlade[c], Jean-Hubert Schmitt[a]

[a] *MSSMat, CNRS, CentraleSupélec, Université Paris-Saclay, 91190 Gif-sur-Yvette, France*
[b] *iMAP, Université Catholique de Louvain, 1348 Louvain-la-Neuve, Belgium*
[c] *ArcelorMital Global R&D - Automotive Products, Maizieres, Voie Romaine, 57583 Maizieres-les-Metz, France*

Abstract

Medium Mn transformation-induced plasticity (TRIP) steels, a subgroup of third generation advanced high-strength steels (AHSS), often present a combination of both dynamic strain aging (DSA) and TRIP. It has been previously shown that TRIP coincides with the passage of strain bands due to DSA, but their interdependence has not been well-established. This study seeks to explore the interactions between the two phenomena as well as the commonly-observed negative strain rate sensitivity. Digital image correlation (DIC) and *in-situ* magnetic measurements of the retained austenite fraction were employed to demonstrate the variations in mechanical behavior with increasing strain rate. Strain rate jump tests provided measurements of the strain rate sensitivity and were combined with either DIC to characterize PLC bands or with magnetic measurements to measure variations in the martensite fraction during the jumps. Finally, the micromechanics defining the peculiar bursts of martensite transformation in response to strain rate jumps are discussed in terms of a competition between dislocation mobility and austenite stability.

Keywords: Dynamic strain aging, PLC, strain rate, strain rate jumps, TRIP, retained austenite, strain rate sensitivity

1. Introduction

The need for high-strength, high-formability steels that are easily weldable is of great importance for automotive manufacturers seeking mass reductions in their products. Twinning-induced plasticity (TWIP) steels provide a significant improvement in both strength and ductility compared to traditional transformation-induced plasticity (TRIP) steels, but are quite difficult to process due to their high alloy content. A recently-developed third generation of advanced high-strength steels (AHSS) provides promising compromise between the two.

Medium manganese steels in particular present higher strength and ductility than conventional first generation TRIP steels, but with a lower alloy content than TWIP steels to facilitate processing. Relying on an intercritical annealing step in the ferrite + austenite domain of the iron-carbon phase diagram, complex microstructures with an ultra-fine grain size (<1 μm) are obtained and result in high work hardening while maintaining some ductility. This is achieved through a composite effect in which ferrite enhances ductility and retained austenite increases the work hardening capacity through the TRIP effect. Optimizing the microstructure to obtain the desired mechanical properties is, however, a nontrivial task as it requires control of both the volume fraction of retained austenite and its stability.

Third generation AHSS sometimes exhibit a negative strain rate sensitivity (SRS), which can greatly reduce the amount of work hardening obtained at high strain rates. This is generally not observed in conventional TRIP steels [1, 2, 3, 4], although it has been reported in austenitic stainless steels [5, 6]. Previous studies show an obvious negative SRS in third generation AHSS [7, 8, 9, 10]. Some authors propose that this is due to stabilization of the retained austenite via adiabatic heating at higher strain rates [5, 11, 12, 13]. In TWIP steels adiabatic heat favors dynamic strain aging (DSA) and negative SRS by facilitating diffusion [14]. As such, the negative SRS could be due

*Corresponding author
Email address: michael.callahan@uclouvain.be (Michael Callahan)

to the instantaneous relaxation and the Portevin-Le Châtelier phenomenon (PLC) rather than decreased martensite transformation.

Compounding the microstructural complexity of these steels is the frequent observation of both static and dynamic strain aging in the form of Lüders or PLC bands [15, 16, 17, 18]. Previous work has related these strain instabilities to the phase transformation during straining in Medium Mn steels [7, 16, 19]. While the community has gained some understanding of the effect of strain aging on mechanical properties in this alloy system, evidence regarding the origins of strain aging remain elusive particularly for dynamic strain aging.

A common hypothesis is that the PLC bands observed in Medium Mn TRIP steels are due to the interaction of C-Mn clusters and partial dislocations, resulting in a pinning effect akin to traditional PLC [3, 17, 18, 20]. Pinning of dislocations by Cottrell atmospheres [21] or by C-Mn clusters depends on the relative velocities of interstitial diffusion and dislocation slip [22], which leads to a range of strain rates for which plasticity is unstable. For these strain rates, deformation occurs through the formation of highly localized strain bands which can be either propagative or static in nature. This form of DSA is often accompanied by a negative strain rate sensitivity and can be avoided during forming by applying sufficiently high strain rates.

In traditional TRIP steels, the strain rate has been observed to either have little effect on mechanical properties or to exhibit a positive SRS [23, 1, 4, 5, 24]. However, the strain hardening rate depends heavily on the kinetics of the martensite transformation during straining. It was noted by several authors [15, 25, 2, 12, 26] that temperature changes in the sample can cause the strain hardening rate to vary significantly. Thus, while the strain rate itself might not affect the TRIP rate, temperature certainly does as was previously demonstrated in isothermal experiments on a classical TRIP steel [27]. Strain rate and DSA have individually been studied in TRIP steels, but the interaction of the two has yet to be clearly explained.

While previous work has shown that the martensite transformation during straining coincides with the passage of PLC bands [7], it is not known whether the PLC bands induce martensite transformation or whether the instantaneous relaxation resulting from the transformation leads to a PLC-type band [28]. Moreover, the observed negative SRS could be related to either DSA or to a reduction in the transformation rate due to adiabatic heat at higher strain rates. Decoupling the DSA and TRIP phenomena is a challenging proposition and makes it difficult to isolate just one of the effects when both are present. This study will seek to employ both strain rate jump tests and a previously-developed magnetic measurement system for austenite volume fraction measurements [7] to attempt to understand the interaction between DSA and the strain-induced martensite transformation.

2. Material and methodology

2.1. Material fabrication

A Medium Mn steel containing 0.2 wt% C, 5 wt% Mn and 2.5 wt% Al was cast and hot-rolled at austenitizing temperature to produce a homogeneous austenitic microstructure, quenched to a fully martensitic structure, and cold-rolled to a thickness of 1.25 mm. Finally, the resulting sheets were annealed in the intercritical ferrite + austenite domain at temperatures of T_{IA}=740°C, T_{IA}=760°C, or T_{IA}=780°C for 2 minutes. During intercritical annealing, the cold-worked martensite is transformed to ferrite and austenite that nucleate at the intersections of martensite laths. This produces an ultra-fine-grained (UFG) mixture of ferrite and retained austenite which is metastable at room temperature. In the case where intercritical annealing was performed at 780°C, a significant fraction of the retained austenite transformed to α' martensite upon cooling to room temperature. The temperature of the intercritical anneal affects the stability and volume fraction of the retained austenite, as demonstrated previously by several groups [29, 30, 31, 17]. In the present work, the microstructures presented in Table 1 were obtained for the corresponding intercritical annealing temperatures. The values of M_s are calculated according to [32]. The reported errors are calculated from the standard error of the XRD and magnetic characterizations. Figure 1 provides examples of the microstructures observed in samples annealed at 740°C and 780°C in both the unstrained state and after straining until fracture.

2.2. Mechanical testing

Tensile dog-bone specimens with an active tensile length of 60 mm and width of 10 mm were cut along the rolling direction of the sheet. Unidirectional tensile tests were performed using an Instron extensometer with a 12.5mm initial

Table 1: Microstructures of the Med Mn TRIP Steel

$T_{IA}(°C)$	$\alpha - ferrite(vol.\%)$	$\gamma - austenite(vol.\%)$	$\alpha' - martensite(vol.\%)$	$M_S(°C)$ **[32]**
740	70± 1.7	30± 1.7	0	-7.5
760	64± 2.5	36± 2.5	0	26
780	68± 0.9	17± 0.9	15± 0.9	58

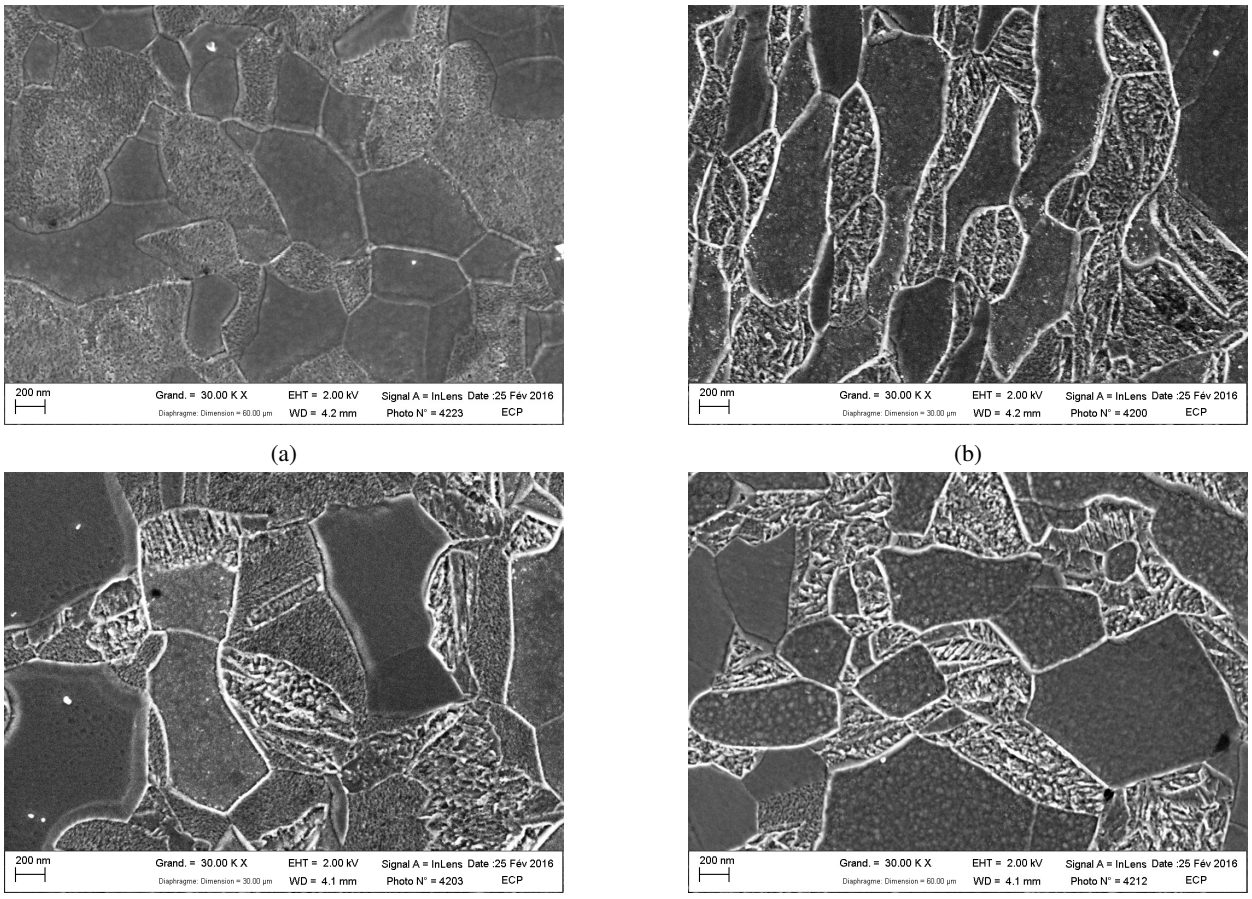

Figure 1: SEM images of the samples annealed at 740°C (a, b) and 780°C (c, d) in the unstrained state (a, c) and after straining until fracture (b, d). Plastic deformation causes retained austenite to transform into martensite at different rates depending on the annealing temperature. In (b), the transformation is only partially complete at fracture but in (d) 100% of the austenite has transformed into martensite due to its lower stability.

length on an MTS hydraulic tensile testing machine. The applied displacement rate of the piston was set such that initial strain rates in the sample were $10^{-4}s^{-1}$ or $10^{-2}s^{-1}$.

Tensile tests were performed both at constant strain rates and with strain rate jumps. The tests were performed with either digital image correlation (DIC) or magnetic measurements of the retained austenite volume fraction. In this way, the strain rate sensitivity (SRS) could be assessed alongside either the band characteristics (when bands are present) or the changes in the the retained austenite volume fraction (martensite transformation rate).

The strain rate jump tests were done in order to characterize the strain rate sensitivity of the samples. The initial strain rate in the sample was $10^{-4}s^{-1}$. This strain rate was maintained until roughly 2-3% strain beyond the end of the Lüders plateau (for samples in which there was a yield point elongation). If no Lüders plateau occurred, the jump was executed 2-3% strain after yielding. Each time a strain rate jump was performed, the strain rate was accelerated to $10^{-2}s^{-1}$ and maintained at this speed for 2 mm of displacement, after which the strain rate returned to $10^{-4}s^{-1}$. The test was then allowed to continue for several percent strain before initiating a second strain rate jump to $10^{-2}s^{-1}$. This pattern of alternating between the two strain rates was repeated until rupture, as illustrated schematically in Figure 2a.

The strain rate sensitivity (SRS) of the material was quantified by calculating both the instantaneous SRS, m_i, and the steady state SRS, m_{ss} as given by [33]:

$$m = \frac{log(\sigma_{x,1}/\sigma_{x,2})}{log(\dot{\epsilon}_{x,1}/\dot{\epsilon}_{x,2})} \tag{1}$$

where x can be either i if the instantaneous SRS is being calculated or ss for the steady state SRS.The determination of the stress and strain values is illustrated in Figure 2b in a purely schematic sense. The extrapolation of the stress is based on a linear fit of the several hundred points before the strain rate jump.

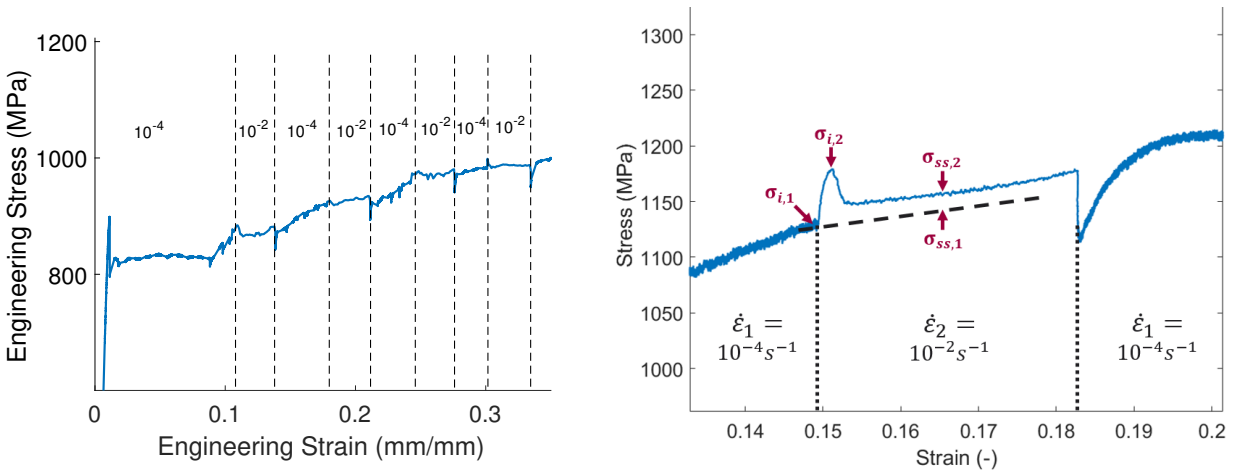

(a) (b)

Figure 2: (a) (T_{IA} = 740°C) The applied strain rate was alternated between $10^{-4}s^{-1}$ and $10^{-2}s^{-1}$ at regular intervals beginning after the complete propagation of the Lüders band. (b) (T_{IA} = 780°C) The instantaneous and steady state strain rate sensitivities, m_i and m_{ss}, were measured by extrapolating the tensile curve at $10^{-4}s^{-1}$ and comparing to the measured behavior at $10^{-2}s^{-1}$ according to Equation 1.

The presence of PLC makes it quite difficult to determine from what point the sample undergoes steady state deformation because the tensile curve is much less smooth than it would be for homogeneous strain. As such, the point at which $\Delta\sigma_{ss}$ is calculated is very important and must be chosen with care. In the current study, it was measured at 0.2% strain after the strain rate jump, 0.5% strain after the jump, and at the midpoint of the period at $\dot{\epsilon} = 10^{-2}s^{-1}$. The difference in each of the results was non-negligible. Due to the transition from a heterogeneous strain regime to a homogeneous strain regime in certain samples (explained later in Section 3.1), the decision was made to use the measurement made at the midpoint of the jump.

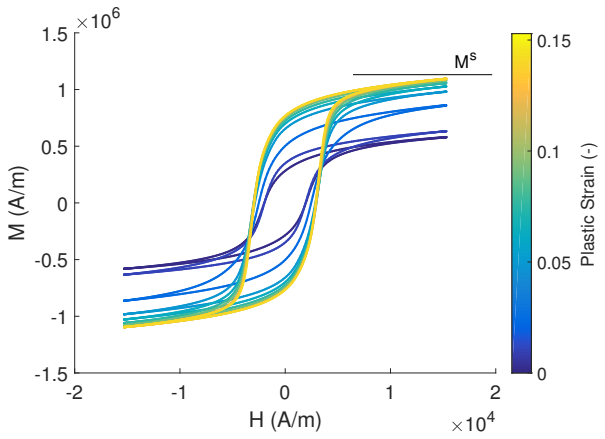

Figure 3: The magnetic method of measuring the retained austenite fraction uses the measured M-H hystereses to calculate the retained austenite fraction from the saturated magnetization M^s, which evolves with plastic strain (represented by the color bar on the right—see online version for references to color) as the transformation progresses.

2.3. Digital image correlation

The samples from sheets annealed at 740°C and 760°C exhibited strain localization in the form of PLC bands [7]. In order to characterize these bands and how they change when the strain rate jump occurs, a subset of the tensile experiments with strain rate jumps were performed with measurements of the strain field on the surface of the samples using DIC. Images for DIC analyses were obtained by painting the polished sample surface with a black and white speckle pattern and DIC images were captured using a pco.1200 high speed camera. 780 × 500px images were captured at 5 frames per second. Two halogen lamps were used to illuminate the specimen surface.

DIC calculations were performed using Correli RT3 using 3-node triangular elements with a regularization length of 50 pixels (~1.85 mm) and an element size of 10 pixels (~0.35 mm) [34]. The regularization applied serves to enforce the mechanical admissibility of the calculated displacement field given a state of unidirectional tension. The incremental strain fields between image n and $n-1$ were used to detect the presence of strain bands when DSA was present. Line profiles were traced over the plotted longitudinal strain fields and the peaks that were produced by strain bands were fitted with Gaussian curves. The full-width at half-max (FWHM) of the Gaussian was used as a metric for the width of the strain band while the center of the Gaussian was used to determine the position of the peak and its displacement between two images. The widths of the bands were corrected for the displacement of the band between two images via their calculated propagation velocities. The width, propagation velocity, strain increment, and strain rate in the band relative to the applied macroscopic strain rate were all used to characterize the strain bands and any changes in these characteristics that occurred when the strain rate was changed during a jump.

2.4. Magnetic measurements of retained austenite fraction

The volume of retained austenite present in each sample was measured *in-situ* during tensile testing using a measurement system previously described in [7]. The measurement method will be briefly summarized here.

A cyclic current is applied to a primary coil placed around the tensile sample, which creates a magnetic field (H) within the coil. This field creates an induced potential in the sample itself based on the quantity of ferromagnetic material that is present. This induction is measured by a 10 mm secondary coil wound around the sample surface and is used to calculate the magnetization (M) in the sample. These data are used to create M-H hystereses from which the value of the magnetization at saturation is extracted (M^S) as shown in Figure 3.

The retained austenite volume fraction is typically measured via the magnetic properties using a simple ratio:

$$f_\gamma = 1 - f_{\alpha+\alpha'} = 1 - \frac{M^s}{M^s_\alpha} \tag{2}$$

where M^s is the measured saturated magnetization and M^s_α is the corresponding value for a purely ferromagnetic material. This formula, however, makes the assumption that the magnetic field applied to the microstructure is homogeneous.

In fact, the high initial proportion of paramagnetic retained austenite in the samples causes a demagnetizing effect in the surrounding ferrite and martensite grains, creating a difference between the local magnetic field in ferromagnetic grains and the macroscopic applied field. The effects of this difference must be taken into account if the measurement of the austenite fraction is to be accurate. This is not typically done in measurements made by ferritescope, but was previously shown to give a significant improvement in measurement precision as compared to X-ray diffraction measurements [7]. The correction used in this study is made by localizing the applied field in the microstructure with an Eshelby model [35]. It uses a modification of the method previously published [7] to remove the need for a phenomenological mixture parameter. Instead, the calculation is reformulated to use a physical parameter: a reference value of the magnetic susceptibility for a purely ferromagnetic sample. Beginning with the solution to the Eshelby problem for the anhysteretic (reversible) magnetic behavior [35, 36]:

$$f_{\alpha+\alpha'} = \frac{\chi\,(3 + 2\chi + \chi_\alpha)}{\chi_\alpha\,(3 + 3\chi)} \tag{3}$$

which can be simplified to:

$$f_{\alpha+\alpha'} = \frac{\chi/\chi_\alpha\,(3/\chi_\alpha + 2\chi/\chi_\alpha + 1)}{3/\chi_\alpha + 3\chi/\chi_\alpha} \tag{4}$$

Where χ is the magnetic susceptibility and χ_α is the susceptibility of a purely ferromagnetic reference sample. By considering that $\chi = \frac{1}{3}A_s\mu_0 M^{s2}$ and $\chi_\alpha = \frac{1}{3}A_s\mu_0 M^{s\,2}_\alpha$, one can express Equation 4 as

$$f_{\alpha+\alpha'} = \frac{(M^s/M^s_\alpha)^2\left(3/\chi_\alpha + 2\,(M^s/M^s_\alpha)^2 + 1\right)}{3/\chi_\alpha + 3\left(M^s/M^s_\alpha\right)^2} \tag{5}$$

This formulation enables the localization of the applied field using only measured hysteretic data, making it possible to perform the measurement *in-situ* without needing to pause the tensile experiment. References values for M^s_α and χ_α are needed however. The reference for M^s_α is taken as $1.3 \times 10^6\ \mathrm{A\,m^{-1}}$ as obtained from samples annealed at 780°C and quenched in liquid nitrogen. The reference value for χ_α is approximated as $\chi_\alpha = \frac{M^s_\alpha}{H_{max}} \approx 114\ \mathrm{A\,m^{-1}}$.

A second correction was made to account for the piezomagnetic coupling known commonly as the Villari effect [37]. As the measurements are to be made under load during tensile testing, the high applied stress will decrease the measured values of M^s significantly and must be corrected. This is accomplished on the basis of a multidomain model developed to simulate the coupled magnetic and mechanical behaviors. Because we are interested only in the value of M^s rather than the whole M-H hysteresis, this model is simplified by application of a second order Taylor expansion. The resulting linear expression applies the magneto-mechanical coupling only to the endpoints of the hysteresis and results in the expression:

$$M^s_\sigma = M^s(1 + \eta\sigma) \tag{6}$$

where M^s_σ is the magnetization measured at a given stress, σ is the applied stress, and η is a physical parameter related to the piezoelectric coefficient. Here, η is on the order of $10^{-5}\ \mathrm{MPa^{-1}}$. This value is fitted such that the magnetization of the sample during unloading remains roughly constant.

When inserted into Equation 5, this gives the final expression that was used to calculate the retained austenite fraction *in-situ* during tensile testing:

$$f_{\alpha+\alpha'} = \frac{(M^s_\sigma/M^s_\alpha)^2\left(3/\chi_\alpha + 2\,(M^s_\sigma/M^s_\alpha)^2 + 1\right)}{3/\chi_\alpha + 3\left(M^s_\sigma/M^s_\alpha\right)^2} \tag{7a}$$

$$f_\gamma = 1 - f_{\alpha+\alpha'} \tag{7b}$$

The magnetic measurements were made continuously during tensile testing for an applied magnetic field cycled at a frequency of 10 Hz. This frequency ensured that the measurement made was volumetric while also providing a very high number of data points that would not be attainable with other methods except for perhaps synchrotron radiation.

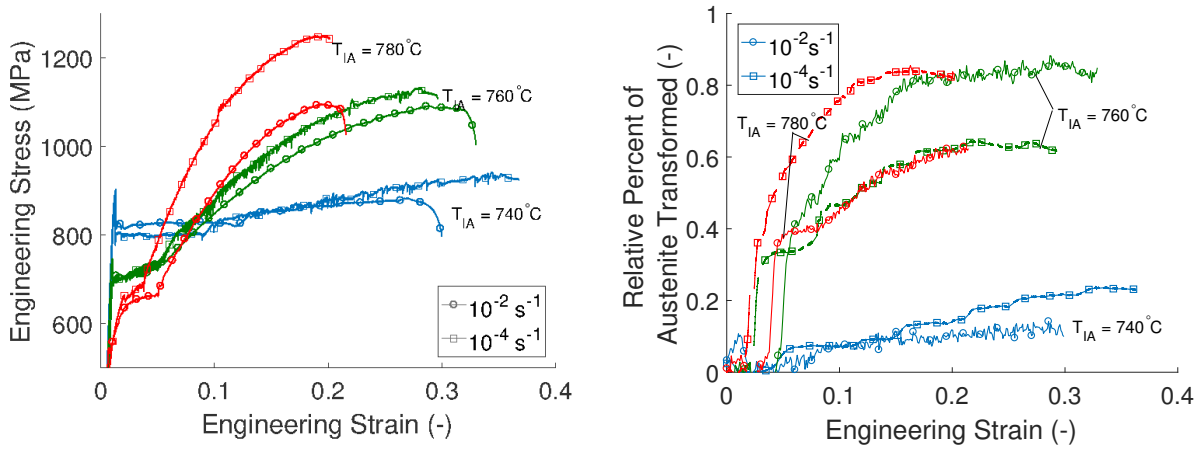

(a) (b)

Figure 4: (a) Tensile behavior for intercritical annealing temperatures of 740°C, 760°C, and 780°C at strain rates of $10^{-4}s^{-1}$ and $10^{-2}s^{-1}$. (b) As shown by evolution of the measured austenite volume fraction, the negative strain rate sensitivity is due to a reduction in martensite transformation caused by adiabatic heating at higher strain rates.

The field was cycled continuously for about 40 s until the buffer of the acquisition card was filled, after which point a new acquisition was started. The data was plotted alongside the tensile data on a common temporal axis to observe changes in the austenite fraction during strain rate jumps and to compare measured austenite fractions with the SRS measured from the jumps.

3. Results

3.1. Tensile behavior and TRIP kinetics

Tensile tests at constant strain rates for each intercritical annealing temperature showed a clear negative strain rate sensitivity, as shown in Figure 4a. Figure 4b shows the fraction of the initial population of retained austenite that has transformed for a given level of strain, which serves to quantify the kinetics of the phase transformation. In samples annealed at 740°C and 780°C, for example, it can be seen that the transformation occurred more slowly for higher strain rates.

In Figure 4 it can be seen that when the strain rate is increased from $10^{-4}s^{-1}$ to $10^{-2}s^{-1}$ in samples annealed at 780°C, the transformation rate decreased. However, in samples annealed at 760°C the transformation rate increased with increased strain rate. The primary difference between the two annealing temperatures is that for annealing at 780°C PLC is never observed, while for 760°C there is PLC at $10^{-4}s^{-1}$ but not at $10^{-2}s^{-1}$. Additionally, in the samples annealed at 740°C where PLC was observed at both strain rates, the transformation rate decreased with strain rate. This could lead one to conclude that there is a relationship between the presence or not of PLC, the transition from a PLC to homogeneous strain domain, and the kinetics of TRIP.

A similar correlation between the martensite transformation and Lüders bands has been observed previously by Steineder *et al.* [38] who used the Ludwigson-Berger model for transformation kinetics [39] to relate transformation rate to the yield point elongations observed in medium Mn steels. The Ludwigson-Berger model, given in Equation 8, is a 2 parameter model that can be reduced to a single parameter in the case of TRIP steels [40]. It is for this reason that it is employed here rather than the Olson-Cohen models [41] commonly used for TRIP steels, although the Olson-Cohen parameters for these alloys were published previously [7].

$$\frac{1}{V_\gamma} - \frac{1}{V_{\gamma,0}} = \frac{k}{p}\varepsilon \tag{8}$$

In Equation 8, $V_{\gamma,0}$ is the initial retained austenite volume fraction, V_γ is the instantaneous austenite fraction, and k and p are model parameters, with p taken as 1 for TRIP steels according to Matsumura *et al.* [40].

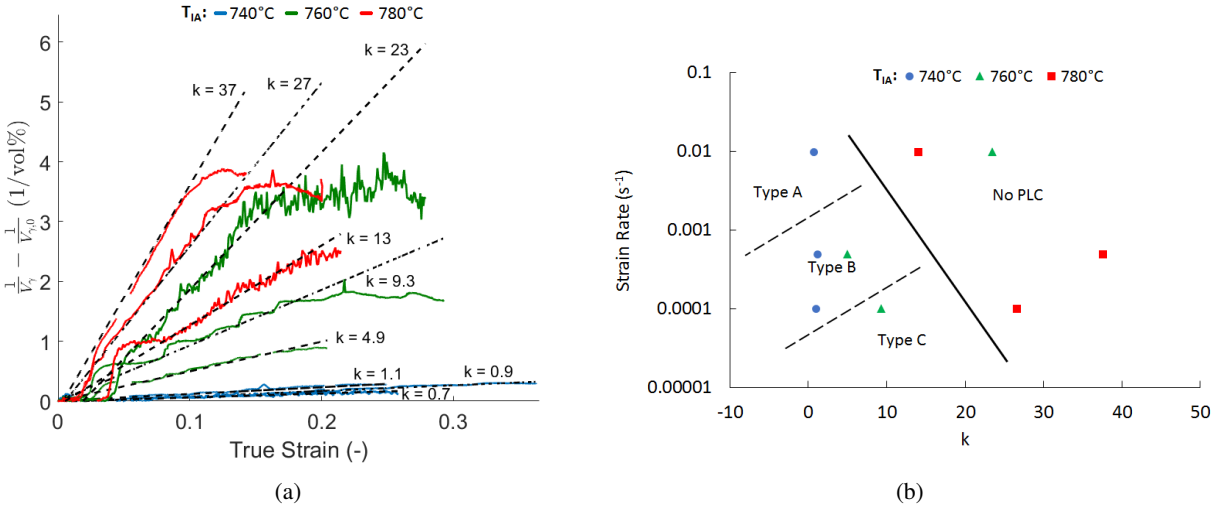

(a) (b)

Figure 5: (a) The Ludwigson-Berger model was applied to transformation kinetics data to quantify transformation rates at different strain rates. (b) This made it possible to create a map of the domains where PLC occurs as a function of strain rate and austenite stability via the parameter k of the L-B model. Data from the previous study using a strain rate of $5 \cdot 10^{-4}\mathrm{s}^{-1}$ is included [7].

Figure 5a shows the transformation kinetics for each annealing temperature and strain rate according to the Ludwigson-Berger model using k as the sole model parameter. From these figures one can observe that above roughly $k = 10 - 12$ PLC is no longer observed, highlighting the correlation between transformation rate and strain instability. Moreover, Figure 5b provides a map indicating the domains in which PLC is observed (as well as the type of PLC [33, 42, 43]) as a function of both strain rate and k. Figure 5b includes data from the previous study using a strain rate of $5 \cdot 10^{-4}\mathrm{s}^{-1}$ [7].

If the observed strain instabilities are a classical PLC originating from interactions between solute clusters and dislocations, the disappearance of strain instabilities with increasing transformation rate could be explained by the generation of mobile dislocations when strain-induced martensite is formed [44]. These new dislocations could allow slip to continue even if many existing dislocations are pinned by solutes.

Alternatively, the strain instability could be a result of the martensite transformation itself if at certain strain rates the martensite transformation rate is too slow to accommodate the strain increment imposed by the macroscopic strain rate. If the transformation rate is too slow, it could be that the strain is localized in a band in order to increase the local strain rate to attain the necessary plastic strain rate. The disappearance of PLC, then, would simply be a result of a transformation rate sufficiently rapid to accommodate the macroscopic strain rate without a need to localize the strain in a band.

3.2. Strain rate sensitivity

The instantaneous strain rate sensitivity as measured from the strain rate jumps produced the expected result: the instantaneous SRS is positive and more or less constant across all samples as seen in Figure 6. The steady state SRS taken at the midpoint of the high strain rate period, is shown in Figure 7a as a function of strain and in Figure 7b as a function of the retained austenite volume fraction. It can be seen that for the lowest levels of strain, the SRS is initially negative and gradually tends towards 0 as strain increases, suggesting that the negative SRS occurs when there is a large volume fraction of austenite. In Figures 6 and 7, the A, B, and C suffixes in the legend simply refer to different samples.

When plotted as a function of the austenite fraction, however, the global trend is that the SRS actually increases with the retained austenite volume fraction. The SRS was negative in samples annealed at 780°C even though no PLC was present, so the PLC bands are not a by-product of negative SRS. Moreover, the SRS was more negative for processing conditions resulting in a less stable austenitic phase. These trends would seemingly support the idea that the negative strain rate sensitivity is a result of stabilization of the retained austenite via adiabatic heating. In the

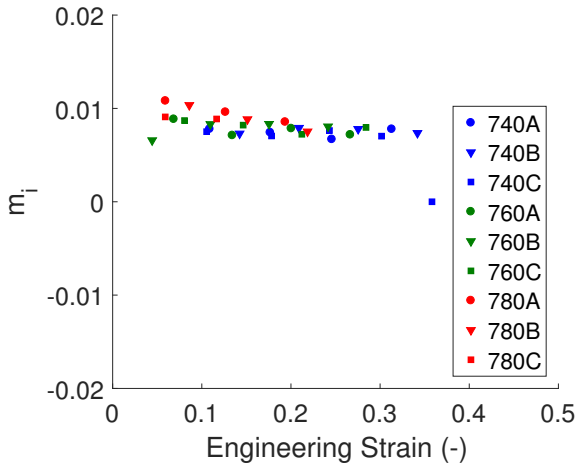

Figure 6: The instantaneous strain rate sensitivity m_i was constant and positive, as expected for most materials.

case of the samples annealed at 740°C, the retained austenite is already relatively stable, so an increase in temperature shouldn't significantly affect the strain hardening obtained and the SRS should not be strongly negative. However the retained austenite in the samples annealed at 780°C is very unstable and a small increase in the temperature of the sample could stabilize it sufficiently to have a noticeable decrease in strain hardening.

Considering each intercritical annealing temperature individually (rather than globally for all T_{IA} as in the previous paragraph), the SRS increased as the austenite fraction decreased. This could correspond to a saturation of the martensite transformation due either to a highly stable austenitic phase or a near-complete transformation of the austenite. Thus, when no more martensite is transforming, the SRS trends away from negative values. In the case of the samples annealed at 780°C, this is not observed, but in that case the austenite transforms very quickly and its low stability likely makes the sample more sensitive to adiabatic heat than the others.

The tensile tests that included strain rate jumps between $10^{-4}s^{-1}$ and $10^{-2}s^{-1}$ showed interesting strain hardening behaviors related to the abrupt changes in strain rate. Figure 8 shows the tensile curves (a,c,e) and the relative fractions of retained austenite transformed to martensite (b,d,f) for each of the three intercritical annealing temperatures. It can be seen that for the samples annealed at 740°C, the strain hardening in the sample on which strain rate jumps were performed was significantly higher than in either sample deformed at a constant strain rate. This is observed in the transformation rate curves as well, where a burst of martensite transformation occurs at the moment of the strain rate acceleration. This burst of transformation exceeds the transformation rate at constant strain rate, perhaps due to the over-stress that occurs at the instant of strain rate acceleration.

A superior transformation rate for samples undergoing strain rate jumps is also observed in samples annealed at 780°C, but in this case the martensite transformation is rapid enough that the samples strained at a constant strain rate of $10^{-4}s^{-1}$ attain the same level of transformation at a strain of about 0.12 as the sample with strain rate jumps after the first jump from $10^{-4}s^{-1}$ to $10^{-2}s^{-1}$. By the time the second jump occurs, the strain hardening has largely saturated and no significant difference in tensile behavior results from the last few percent of austenite transformation that occurs.

In the samples annealed at 760°C, a transition from a domain in which strain is heterogeneous to a domain in which strain is homogeneous is observed for constant strain rates. In this case, it is difficult to directly compare the transformation rates because there is no local strain measurement during the magnetic measurements and so the strain calculated from the crosshead displacement must be used. This means that for a strain rate of $10^{-2}s^{-1}$, the strain measured is accurate because the strain in the sample is homogeneous (for annealing at 760°C). However for a strain rate of $10^{-4}s^{-1}$, there is some error in the strain because the macroscopic strain is measured rather than the strain in the band. This means that the local transformation rate is being compared to the macroscopic strain. In samples annealed at 780°C this is not as problematic, as both strain rates give the same deformation conditions regarding strain homogeneity, so a direct comparison is possible. In samples annealed at 740°C, this error due to the presence of strain bands occurs at both strain rates. As such it is inconsequential when one wishes simply to compare the results for

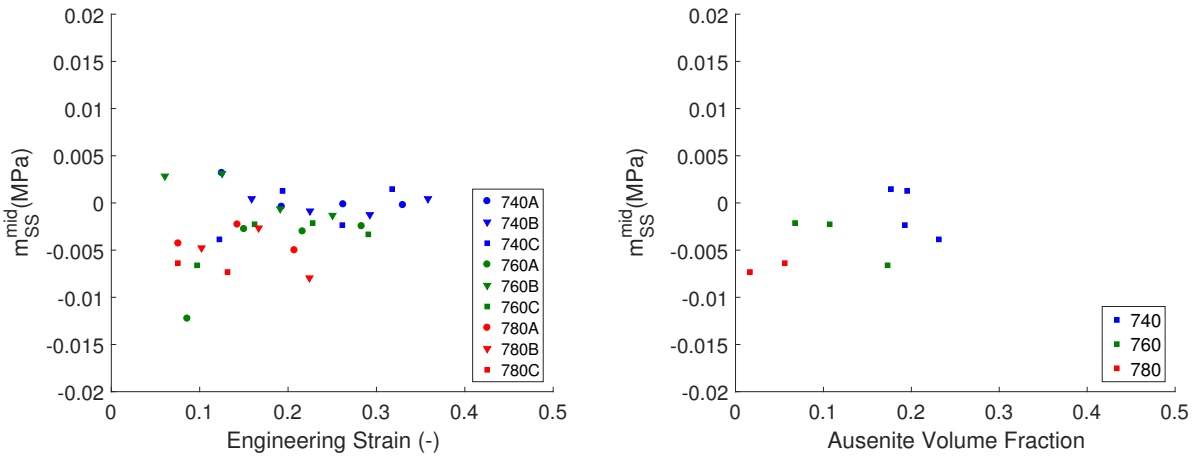

(a) (b)

Figure 7: (a) The steady state SRS was initially negative and tended towards 0 as strain progressed. This was true independently of the presence or not of PLC in the sample. (b) When plotted as a function of the austenite volume fraction for samples upon which magnetic measurements were made, a global trend where m_{ss} increases with V_γ is observed, however when considering individual annealing temperatures it seems that m_{ss} decreases with V_γ when PLC is present.

both strain rates relative to each other.

It would seem that the transformation rate for samples annealed at 760°C initially follows that for a constant strain rate of $10^{-4}s^{-1}$ as expected. When the strain rate jump occurs, the transformation rate attempts to accelerate to the rate that occurs at a constant strain rate of $10^{-2}s^{-1}$. The tensile behavior shows a very slightly higher hardening rate than for either of the constant strain rates. There is no significant difference in macroscopic mechanical behavior between the constant strain rates or the strain rate jump tests. However, the transformation rate does show some variation with strain rate, indicating it could be related to the macroscopic strain rate sensitivity.

3.3. Relation of strain bands, TRIP, and strain rate jumps

While performing strain rate jumps when strain bands are present, the characteristics of the bands should change alongside the strain rate. The question is which characteristics are changed and by how much, as changes to the band width, propagation velocity, or the strain rate in the band will likely have different effects on the martensite transformation.

The changes in the strain bands were observed during DIC experiments and are summarized in Figure 10. The band widths reported are corrected using the band propagation velocities, so the standard error of the width measurements are compounded with those of the velocities which led to high variability particularly for strain bands appearing at strain rates of $10^{-2}s^{-1}$. This makes it difficult to draw a clear conclusion about the band widths, however the velocities and the strain rates in the bands relative to the applied strain rate showed interesting results.

The fact that a band exists in the sample annealed at 760°C after a jump to a strain rate of $10^{-2}s^{-1}$ is perhaps unexpected as the strain is supposed to be homogeneous at this strain rate. In fact, when closely examining the tensile data at the strain rate jump there is a "pseudo-Lüders" plateau that appears at constant stress right after the strain rate jump. Figure 9 provides an example of this phenomenon. The "pseudo-Lüders" plateau corresponds to the strain band that was created at $10^{-4}s^{-1}$ rapidly completing its propagation across the sample (as observed by DIC), after which point the strain can homogenize and deformation continues as it would if the strain rate were constant. It is this band that is characterized in Figure 10 for at T_{IA} = 760°C and a strain rate of $10^{-2}s^{-1}$.

It appears that the propagation velocity of the band increases by about 30-50x when the strain rate is accelerated by 100x. The rest of the strain rate difference should be accommodated otherwise, either by an increase in band width or an intensification of the strain in the band. To more clearly see whether a strain intensification occurred or not, the strain rates in the band reported in Figure 10 are normalized by the initial strain rate of $10^{-4}s^{-1}$. It is clear that in samples annealed at 740°C, at the strain rate jump the strain rate in the band increases by about 25x relative to the

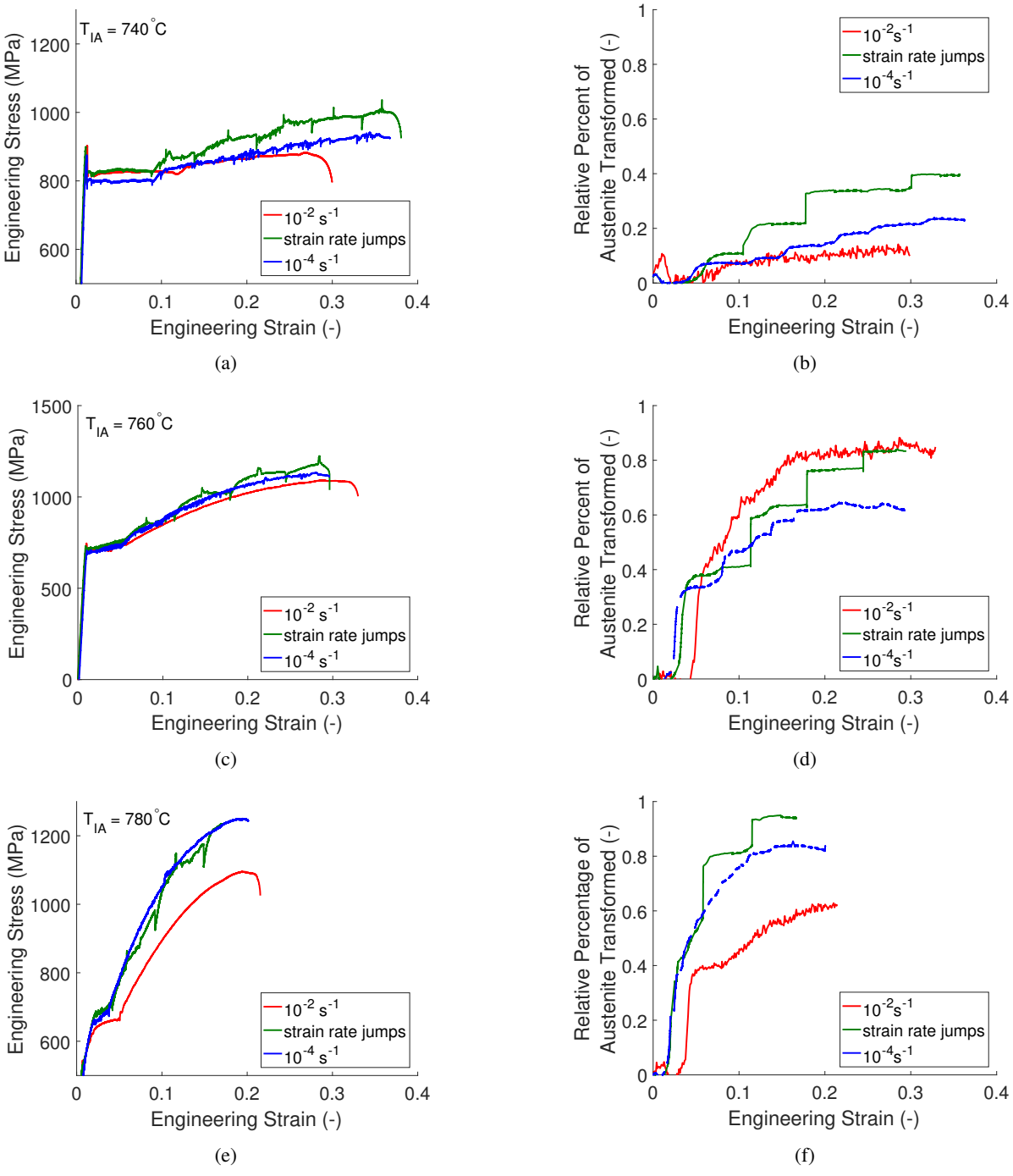

Figure 8: When strain rate jumps are employed, it can be seen in tensile data (a-c) that the ultimate strength can increase when PLC is present. There is also a difference in the transformation rates (d-f) where bursts of transformation occur during strain rate jumps. It appears that the strain rate jumps result in overall faster transformation than is seen at constant strain rates, with the exception of the samples annealed at 760°C. These exhibit some peculiar behavior due to the transition from a PLC regime to a homogeneous strain regime.

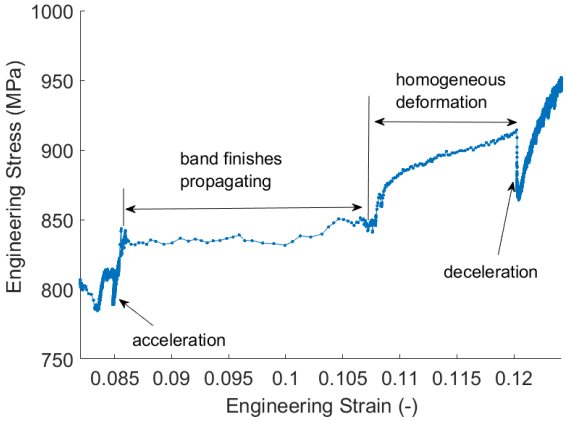

Figure 9: In the sample annealed at 760°C, PLC is present at $10^{-4}s^{-1}$ but strain is homogeneous at $10^{-2}s^{-1}$. When a strain rate jump is executed, the pre-existing PLC band that formed at $10^{-4}s^{-1}$ rapidly completes its propagation. Once the band has fully traversed the sample; strain continues homogeneously.

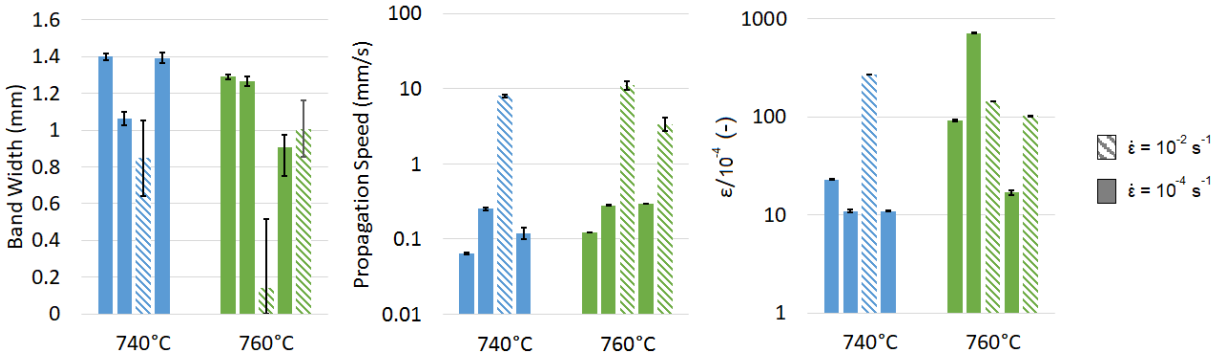

Figure 10: The width, propagation speed, and strain rate in the band normalized by the slowest strain rate of $10^{-4}s^{-1}$ are plotted for each successive band in two samples annealed at 740°C and 760°C. The band width doesn't show a clear difference between the two strain rates, however the propagation speed increased by 30-50x its value at $10^{-4}s^{-1}$. In the sample annealed at 740°C the strain rate in the band was significantly higher when the strain rate was accelerated. In the sample annealed at 760°C, however, the strain rate in the band was roughly the same as at low strain rate. This is because the dislocation velocity in the band is sufficiently high when the strain rate jump is applied and because at $10^{-2}s^{-1}$ homogeneous strain is favored in this sample.

strain rate in the band at $10^{-4}s^{-1}$. This does not seem to occur in samples annealed at 760°C, however, as the strain rate in the band upon accelerating to $10^{-2}s^{-1}$ is more or less the same as it was at $10^{-4}s^{-1}$.

Furthermore, if the magnetic data and tensile data during strain rate jumps are examined side by side as in Figure 11, another unusual result is observed. In samples annealed at 740°C and 780°C, there is a burst of martensite transformation that occurs at the moment the strain rate is accelerated. After this burst, no further transformation occurs until after the strain rate is again decelerated and straining continues at $10^{-4}s^{-1}$. This trend was systematic for all strain rate jumps in different samples during several experiments. Paradoxically, the samples annealed at 760°C exhibited the opposite behavior. At the instant of the strain rate jump, there is no burst of transformation. Rather, no transformation occurs at all until after the moment of deceleration when a burst of transformation finally appears.

4. Discussion

In order to clarify the relationships between strain rate, transformation rate, and the peculiar bursts of martensite transformation that were observed, it is necessary to understand what happens in the microstructure at the moment of a strain rate jump. The explanation of these relationships necessitates, in turn, an explanation of the means by which

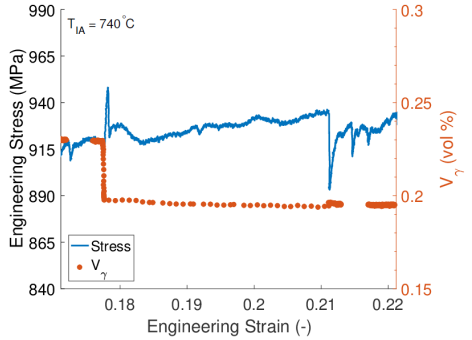

(a)

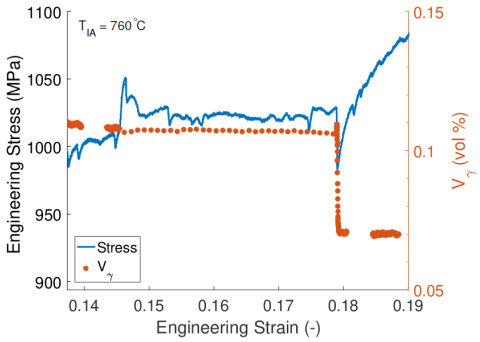

(b)

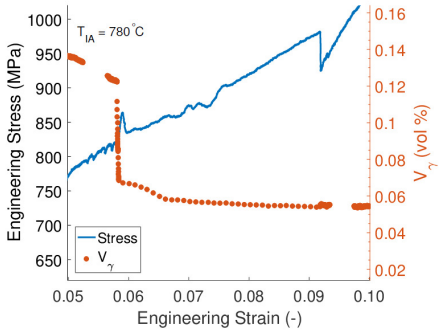

(c)

Figure 11: When strain rate jumps were applied, a sudden burst of martensite transformation was measured. In samples where the stability of PLC was the same at both strain rates (a,c), this burst occurred upon accelerating the strain rate. Curiously, when jumping from a PLC regime to a homogeneous strain regime, the burst occurred upon deceleration. This is attributed to a competition between dislocation velocity and the creation of mobile dislocations during TRIP. The mechanism that is selected to accommodate the strain rate acceleration will determine when the burst of transformation occurs.

a sudden strain rate change is accommodated by the microstructure. In the beginning of this section, a foundation will be laid for understanding the roles of dislocation motion and martensite nucleation in determining the local strain rate. After this, explanations will be proposed for the behaviors observed for each intercritical annealing temperature and in particular for the bursts of martensite transformation.

The plastic strain rate can be related to the mean velocity of mobile dislocations via [45]:

$$\varepsilon = \rho b L \tag{9}$$

where ρ is the density of mobile dislocations, L is the free mean path, and b is the Burgers vector.

Dislocation slip is initiated when a certain minimum stress is achieved. This stress is determined by either the stress necessary to activate or create dislocation sources or by the unpinning stress in the case of the Cottrell model. In either case, there is a waiting time t_w related to the local stress rate that defines the time needed to attain the minimum stress for dislocation slip. It has been shown that the waiting time is inversely proportional to the strain rate [46], so Equation 9 can be differentiated to obtain:

$$\dot{\varepsilon} = \rho b \bar{v} + \dot{\rho} b L \tag{10}$$

where $\bar{v}$ is the average velocity of mobile dislocations. The wait time t_w is implicitly accounted for in $\bar{v} = {}^{L}/_{t_w}$.

The martensite transformation will also contribute to the strain rate through the plastic strain it induces. The magnitude of this contribution depends on the martensite nucleation rate $\dot{f}_m$ which can be obtained from, for example, Olson and Cohen's description of the martensitic transformation rate [41]. The effects of the martensite transformation can be accounted for in Equation 10 by adding in another term:

$$\dot{\varepsilon} = \rho b {}^{L}/_{t_w} + \dot{\rho} b L + \dot{f}_m \Delta\varepsilon_{\gamma\rightarrow\alpha'} \tag{11}$$

In this expression, $\dot{f}_m$ is the product of the density of martensite nucleation sites and the probability of nucleation of martensite. This probability is not a fixed value, but varies depending on the type of site (dislocation intersection, shear band intersection, etc) and local composition of the parent austenite grain, among other factors. Thus the probability of transformation follows a statistical distribution, leading to a progressive transformation of austenite to martensite. This is observed, for example, during the cooling of TRIP steels when no new nucleation sites are formed, but a gradual transformation occurs between the martensite start, M_s, and finish M_f temperatures.

When plastic strain is present through an applied strain rate $\dot{\varepsilon}$, both the rate of generation of nucleation sites and the probability of nucleation are affected. It has been shown that increasing the applied strain rate increases the number of nucleation sites through the creation of additional shear bands [6]. The probability of transformation initially is increased for higher strain rates, but then decreases possibly due to adiabatic heat generation [6, 47]. An important observation is that the martensite transformation does not require any incubation time and can begin immediately upon initiation of a strain rate jump [47]. Additionally, the plastic strain increment associated with the transformation results in an instantaneous local softening before the hardening effect of the transformed martensite manifests [48].

With this understanding of the relationships between strain rate, dislocation motion, and the martensite transformation in mind, three cases will be considered in the subsections to follow. They are organized according to the homogeneity or heterogeneity of strain for each macroscopic strain rate. First is the case for the samples annealed at 780°C where the initially homogeneous deformation remained homogeneous at high strain rate. Next, the samples annealed at 740°C where PLC bands existed at both strain rates are discussed. Finally, the samples annealed at 760°C are considered, where the strain rate jump causes a transition from a PLC regime to a homogeneous strain regime. The behaviors of each will be explained on the basis of the selection of the deformation mechanism needed to accommodate the increased strain rate.

4.1. T_{IA} =780°C: homogeneous strain at both strain rates

In a material that deforms homogeneously, this selection is based on whether it is easier to activate or create new dislocation sources or to transform austenite to martensite and generate new mobile dislocations in the surrounding grains. In the samples annealed at 780°C, the austenite is very unstable and the energy barrier for transformation is small. As previously mentioned, the waiting time for dislocation slip should decrease at increased strain rate, but this cannot happen instantaneously. Either higher stresses are needed to activate dislocation sources or, in the case of the

Cottrell model, the local solute concentration needs to stabilize before slip can occur [46]. However, the martensite transformation is possible as it requires no wait time before initiating the phase transformation and the probability of martensite nucleation is initially higher when the strain rate is accelerated. Thus, a burst of martensite transformation occurs in order to accommodate the new strain rate. This happens homogeneously throughout the sample.

The population of austenite grains that will be able to transform due to an increment in mechanical work depends on their stabilities. The retained austenite in a steel has a distribution of stabilities due to variations in grain size, crystal orientation relative to the loading direction, and local variations in composition. Additionally, the transformation is sometimes a partial one as the transformation of part of a grain to martensite reduces the volume of the remaining austenite grain, and this size reduction increases the stability of the remaining portion of the grain.

After the strain rate jump is executed and the burst of transformation occurs, all of the austenite grains with a stability that would be transformable at the current mechanical state have already been transformed, so no phase transformation occurs until higher stresses and plastic strains are attained to create new nucleation sites and activate them.

Upon decelerating, the wait time for dislocation slip increases. Dislocation slip continues as normal for the new strain rate and the martensite transformation is once again activated when the stress increases enough to trigger it on new martensite nuclei.

4.2. T_{IA} =740°C: heterogeneous strain at both strain rates

When considering the case where deformation is no longer homogeneous and PLC is present, as in the samples annealed at 740°C, the same logic may be applied. If the dislocation velocity in the existing PLC band is too slow to accommodate the strain rate acceleration, then a burst of martensite transformation occurs instead. This burst occurs systematically each time the strain rate is accelerated. If the transformation occurred only in the strain band, then this would mean that the band was exactly in the zone of magnetic measurement (which was roughly 16% of the sample's tensile length) each time a strain rate jump was performed. The likelihood of the band being at exactly the right position each time is rather small, so one could conclude that the burst of transformation actually occurs homogeneously in the whole volume of the sample. As in the case where deformation was homogeneous, the burst of transformation consumes a certain population of austenite grains and higher levels of stress and strain are needed to continue the transformation.

4.3. T_{IA} =760°C: transition from heterogeneous to homogeneous strain

In contrast to the previously described samples, the samples annealed at 760°C showed a transition from a domain in which PLC bands are present at strain rate of $10^{-4}s^{-1}$ to a domain in which there strain field is homogeneous at $10^{-2}s^{-1}$. The strain rate jump tests on these samples showed the opposite behavior of the other samples, with a burst of transformation upon deceleration rather than acceleration. Some questions arise from this observation: why is there no burst at the moment of the strain rate jump like in the other samples, why is there no transformation during the period at $10^{-2}s^{-1}$, and why does the burst instead occur at deceleration?

First, the lack of transformation upon accelerating the strain rate should be considered. Following the preceding logic, either the acceleration or creation of new mobile dislocations is needed in order to accommodate the increased strain rate. This selection depends on the strain rate in the band (and thus the average dislocation velocity in the band) just before the strain rate jump is executed.

At an applied strain rate of $10^{-4}s^{-1}$, the strain rate in the PLC bands was observed to be roughly $10^{-2}s^{-1}$ in samples annealed at 760°C, as shown in Figure 10. The strain rate in bands observed at $10^{-2}s^{-1}$ was roughly the same as the bands at the lower strain rate and, critically, is the same as the applied macroscopic strain rate after the jump. This is a stark difference from the samples annealed at 740°C where the strain rate in the band increased proportionally to the applied strain rate when the strain rate jump was performed. Upon accelerating, the strain rate in the band was already equal to $10^{-2}s^{-1}$ and was thus sufficient to accommodate the increased macroscopic strain rate. Thus the same band that formed at $10^{-4}s^{-1}$ remained when the strain rate was accelerated to $10^{-2}s^{-1}$ and only its propagation velocity and width increased. Once the band completed its propagation, the strain field homogenized because the change in strain rate had already been accommodated. It continued to deform homogeneously as it would have at a constant strain rate.

The lack of any phase transformation during the period of high strain rate is perhaps unexpected. If it were an effect of adiabatic heat, this would imply that the transformation can begin again once this heat dissipates, meaning

that in these experiments the heat was sufficiently dissipated systematically and exactly at the moment of deceleration where the burst of martensite transformation occurs. This is unlikely, because it would require the band to be in a very precise location with a very precise propagation velocity such that the time for dissipation is the same during each strain rate jump. However, it was shown that adiabatic heat may not be the only contribution to the decreased transformation rate at higher strain rates and that the nucleation itself could have a negative strain rate sensitivity [47]. In any case, because plastic deformation is occurring at high strain rate, new nucleation sites are being creating at this strain rate even if no transformation occurs.

The absence of TRIP during the period of high strain rate is notable in that it shows that TRIP is not necessary for a band to continue propagating. This does not preclude that the martensite transformation could possibly be responsible for the formation of the band initially, but it clearly demonstrates that PLC bands can exist and propagate without any phase transformation. The two effects interact, and TRIP likely accelerates the strain rate in the band, but the two phenomena do not seem to be co-dependent.

Upon decelerating, the waiting time for dislocation motion increases and the dislocations are once again pinned by solutes, as the strain rate returns to an unstable domain. The unpinning of dislocations requires a barrier of mechanical energy to be overcome in order to begin dislocation slip. However, the sample just underwent several percent of plastic strain with no martensite transformation, meaning that significant numbers of martensite nucleation sites were created but not activated. The burst of phase transformation occurs at the moment of deceleration because the mechanical energy needed to transform these nuclei is inferior to the energy needed to unpin the dislocations. Finally, a new PLC band forms. Its formation could be due either because the unpinning stress is attained (in the case of traditional PLC) or because of heterogeneities caused by the formation of martensite. After the PLC band has formed, deformation continues as normal for a strain rate of $10^{-4}s^{-1}$.

5. Conclusions

This study used both digital image correlation and *in-situ* magnetic measurements of the retained austenite volume fraction to examine the interactions between strain instabilities and martensite transformation in a 3rd generation Medium Mn TRIP steel. Strain rate jump tests allowed an assessment of the strain rate sensitivity and, in conjunction with DIC and magnetic results, provided insights into the origins of the negative SRS. Additionally, the domains of stability for the Portevin-le-Châtelier phenomenon were established as a function of strain rate and retained austenite stability. The primary conclusions of the work are as follows:

1. The negative strain rate sensitivity in Medium Mn TRIP steels is an effect of adiabatic heat stabilizing the retained austenite and thus reducing the work hardening rate. The negative SRS is not directly related to DSA, as the SRS was lowest in samples that did not exhibit DSA.
2. There is a clear effect of the austenite stability on the domain in which PLC exists in these alloys. A map defining the ranges of strain rates and austenite stabilities was presented. The austenite stability is quantified using the single-parameter Ludwigson-Berger transformation kinetics model. A more rapid martensite transformation decreases the minimum strain rate needed to obtain homogeneous strain, similar to a decrease in test temperature. This can be explained by the creation of mobile dislocations when martensite transformation occurs, facilitating plasticity despite the existing dislocations being pinned by solutes.
3. During strain rate jump tests, one effect of the acceleration of the strain rate from $10^{-4}s^{-1}$ to $10^{-2}s^{-1}$ was an increase in the propagation velocity of PLC bands. In samples annealed at 740°C where PLC was present at both strain rates, the strain rate in the band also increased. In samples annealed at 760°C where PLC is only present at $10^{-4}s^{-1}$, the strain rate in the band remained the same when the strain rate was accelerated and the strain homogenized once the band completed its propagation.
4. The behavior of the material at the moment of the strain rate jump–namely, the mechanism by which the sudden acceleration is accommodated–is determined by a competition between the activation or creation of new dislocation sources and the activation of the martensite transformation. If the velocity of mobile dislocations is too slow to accommodate the strain rate acceleration, then a burst of martensite transformation will occur when the strain rate jump is executed. This burst of transformation is homogeneous in the active tensile volume and serves to create a population of mobile dislocations to accommodate the acceleration of the strain rate.

5. A particular case was observed in samples annealed at 760°C where the burst of martensite transformation occurred upon deceleration of the strain rate rather than at acceleration as in the other samples. This was explained by a sufficiently rapid dislocation velocity within a PLC band at the moment of the strain rate acceleration, followed by a period at high strain rate during which martensite nucleation sites were created but not activated. Upon deceleration, dislocations are pinned and the energy barrier to activate the nucleation sites is lower than the barrier to unpin dislocations, so a martensite transformation burst occurs and then strain continues normally.
6. Because in the samples annealed at 760°C there are PLC bands present at $10^{-2}s^{-1}$ and no martensite transformation was detected during the periods at high strain rate, it can be concluded that the martensite transformation is not necessary for band propagation. This does not preclude a role of the martensite transformation in band formation however.

Acknowledgements

The authors would like to thank Dr. Denis Solas from Université Paris Sud for his expertise with XRD measurements, Drs. Olivier Hubert and François Hild for their help with magnetic measurements and DIC respectively, and Drs. David Embury and Pascal Jacques for useful discussions of the results obtained.

This study has been performed within the framework of the ANR 13-RMNP-0002 MedMnAl Steels funded by the Agence Nationale de la Recherche (ANR). This project is supported by the competitive cluster "Materalia".

Data Availability

The data used in this study is available from the corresponding author pending approval from the industrial partners involved in the study.

References

[1] F. Ozturk, A. Polat, S. Toros, R. C. Picu, Strain Hardening and Strain Rate Sensitivity Behaviors of Advanced High Strength Steels, Journal of Iron and Steel Research International 20 (2013) 68–74.
[2] S. Curtze, V. T. Kuokkala, M. Hokka, P. Peura, Deformation behavior of TRIP and DP steels in tension at different temperatures over a wide range of strain rates, Materials Science and Engineering A 507 (2009) 124–131.
[3] A. Müller, C. Segel, M. Linderov, A. Vinogradov, A. Weidner, H. Biermann, The PortevinLe Châtelier Effect in a Metastable Austenitic Stainless Steel, Metallurgical and Materials Transactions A: Physical Metallurgy and Materials Science 47 (2016) 59–74.
[4] A. S. Khan, M. Baig, S. H. Choi, H. S. Yang, X. Sun, Quasi-static and dynamic responses of advanced high strength steels: Experiments and modeling, International Journal of Plasticity 30-31 (2012).
[5] J. Van Slycken, P. Verleysen, J. Degrieck, J. Bouquerel, B. C. De Cooman, Dynamic response of aluminium containing TRIP steel and its constituent phases, Materials Science and Engineering A 460-461 (2007) 516–524.
[6] S. S. Hecker, M. G. Stout, K. P. Staudhammer, J. L. Smith, Effects of Strain State and Strain Rate on Deformation-Induced Transformation in 304 Stainless Steel: Part I. Magnetic Measurements and Mechanical Behavior, Metallurgical Transactions A 13 (1982) 619–626.
[7] M. Callahan, O. Hubert, F. Hild, A. Perlade, J. H. Schmitt, Coincidence of strain-induced TRIP and propagative PLC bands in Medium Mn steels, Materials Science and Engineering A (2017).
[8] H. K. Yang, Z. J. Zhang, Y. Z. Tian, Z. F. Zhang, Negative to positive transition of strain rate sensitivity in Fe-22Mn-0.6C-x(Al) twinning-induced plasticity steels, Materials Science and Engineering A 690 (2017) 146–157.
[9] J. Min, L. G. Hector, L. Zhang, L. Sun, J. E. Carsley, J. Lin, Plastic instability at elevated temperatures in a TRIP-assisted steel, Materials and Design 95 (2016) 370–386.
[10] T. A. Lebedkina, M. A. Lebyodkin, J. Chateau, A. Jacques, S. Allain, On the mechanism of unstable plastic flow in an austenitic FeMnC TWIP steel, Materials Science & Engineering A 519 (2009) 147–154.
[11] B. B. He, H. W. Luo, M. X. Huang, Experimental investigation on a novel medium Mn steel combining transformation-induced plasticity and twinning-induced plasticity effects, International Journal of Plasticity 78 (2016) 173–186.
[12] A. A. Tiamiyu, A. G. Odeshi, J. A. Szpunar, Multiple strengthening sources and adiabatic shear banding during high strain-rate deformation of AISI 321 austenitic stainless steel: Effects of grain size and strain rate, Materials Science and Engineering A 711 (2018) 233–249.
[13] X. Wei, R. Fu, L. Li, Tensile deformation behavior of cold-rolled TRIP-aided steels over large range of strain rates, Materials Science and Engineering A 465 (2007) 260–266.
[14] O. Majidi, B. D. Cooman, F. Barlat, M.-G. Lee, Y. P. Korkolis, Thermomechanical response of a twip steel during monotonic and non-monotonic uniaxial loading, Materials Science and Engineering: A 674 (2016) 276 – 285.
[15] L. Luo, W. Li, L. Wang, S. Zhou, X. Jin, Tensile behaviors and deformation mechanism of a medium Mn-TRIP steel at different temperatures, Materials Science and Engineering A 682 (2017) 698–703.
[16] M. M. Wang, C. C. Tasan, D. Ponge, D. Raabe, Spectral TRIP enables ductile 1.1 GPa martensite, Acta Materialia 111 (2016) 262–272.

[17] P. J. Gibbs, E. De Moor, M. J. Merwin, B. Clausen, J. G. Speer, D. K. Matlock, Austenite stability effects on tensile behavior of manganese-enriched- austenite transformation-induced plasticity steel, Metallurgical and Materials Transactions A: Physical Metallurgy and Materials Science 42 (2011) 3691–3702.
[18] S. Lee, B. C. De Cooman, Effect of the Intercritical Annealing Temperature on the Mechanical Properties of 10Pct Mn Multi-phase Steel, Metallurgical and Materials Transactions A 45 (2014) 5009–5016.
[19] B. Sun, N. Vanderesse, F. Fazeli, C. Scott, J. Chen, P. Bocher, M. Jahazi, S. Yue, Discontinuous strain-induced martensite transformation related to the Portevin-Le Chatelier effect in a medium manganese steel, Scripta Materialia 133 (2017) 9–13.
[20] Z. Cai, H. Ding, R. Misra, Z. Ying, Austenite stability and deformation behavior in a cold-rolled transformation-induced plasticity steel with medium manganese content, Acta Materialia 84 (2015) 229–236.
[21] A. H. Cottrell, B. A. Bilby, Dislocation theory of yielding and strain ageing of iron, Proceedings of the Physical Society. Section A 62 (1949) 49.
[22] C. Fressengeas, A. Beaudoin, M. Lebyodkin, L. Kubin, Y. Estrin, Dynamic strain aging: A coupled dislocationsolute dynamic model, Materials Science and Engineering: A 400-401 (2005) 226 – 230.
[23] H. Huh, S. B. Kim, J. H. Song, J. H. Lim, Dynamic tensile characteristics of TRIP-type and DP-type steel sheets for an auto-body, International Journal of Mechanical Sciences 50 (2008) 918–931.
[24] R. Alturk, W. E. Luecke, S. Mates, A. Araujo, K. Raghavan, F. Abu-Farha, Rate effects on transformation kinetics in a metastable austenitic stainless steel, Procedia Engineering 207 (2017) 2006–2011.
[25] J. A. Jiménez, M. Carsí, O. A. Ruano, G. Frommeyer, Effect of testing temperature and strain rate on the transformation behaviour of retained austenite in low-alloyed multiphase steel, Materials Science and Engineering A 508 (2009) 195–199.
[26] N. J. Wengrenovich, G. B. Olson, Optimization of a TRIP steel for adiabatic fragment protection, Materials Today: Proceedings 2 (2015) S639–S642.
[27] A. Rusinek, J. R. Klepaczko, Experiments on heat generated during plastic deformation and stored energy for TRIP steels, Materials and Design 30 (2009) 35–48.
[28] G. B. Olson, M. Azrin, Transformation Behavior of TRIP Steels, Technical Report, AMMRC, Watertown, MA, 1977.
[29] S. Lee, B. C. De Cooman, Tensile Behavior of Intercritically Annealed Ultra-Fine Grained 8% Mn Multi-Phase Steel, Steel Research International 86 (2015) 1170–1178.
[30] R. Wei, M. Enomoto, R. Hadian, H. S. Zurob, G. R. Purdy, Growth of austenite from as-quenched martensite during intercritical annealing in an Fe-0.1C-3Mn-1.5Si alloy, Acta Materialia 61 (2013) 697–707.
[31] a. Arlazarov, M. Gouné, O. Bouaziz, A. Hazotte, G. Petitgand, P. Barges, Evolution of microstructure and mechanical properties of medium Mn steels during double annealing, Materials Science and Engineering A 542 (2012) 31–39.
[32] S. M. C. van Bohemen, Bainite and martensite start temperature calculated with exponential carbon dependence, Materials Science and Technology 28 (2012) 487–495.
[33] X. Bian, F. Yuan, X. Wu, Correlation between strain rate sensitivity and characteristics of Portevin-LeChâtelier bands in a twinning-induced plasticity steel, Materials Science and Engineering A 696 (2017) 220–227.
[34] Z. Tomicevc, F. Hild, S. Roux, Mechanics-aided digital image correlation, The Journal of Strain Analysis for Engineering Design 48 (2013) 330–343.
[35] J. Eshelby, The determination of the elastic field of an ellipsoidal inclusion, and related problems, Proceedings of the Royal Society (1957).
[36] F. Mballa-Mballa, O. Hubert, S. Lazreg, P. Meilland, Multidomain modelling of the magneto-mechanical behaviour of dual-phase steels, in: 18th World Conference on Nondestructive Testing, April, pp. 16–20.
[37] D. Vanoost, S. Steentjes, J. Peuteman, G. Gielen, H. D. Gersem, D. Pissoort, Magnetic hysteresis at the domain scale of a multi-scale material model for magneto-elastic behaviour, Journal of Magnetism and Magnetic Materials 414 (2016) 168–179.
[38] K. Steineder, D. Krizan, R. Schneider, C. Béal, C. Sommitsch, On the microstructural characteristics influencing the yielding behavior of ultra-fine grained medium-Mn steels, Acta Materialia (2017).
[39] J. Ludwigson, J. Berger, J. Iron Steel Inst (1969) 63–69.
[40] O. Matsumura, Y. Sakuma, H. Takechi, TRIP and its Kinetic Aspects in Austempered 0.4C-1.5si-0.8Mn Steel, Scripta Materialia 21 (1987) 1301–1306.
[41] G. Olson, M. Cohen, Kinetics of Strain-Induced Martensitic Nucleation, Metallurgical Transactions A 6 (1975) 791–795.
[42] P. Zavattieri, V. Savic, L.G. Hector Jr., J.R. Fekere, W. Tong, Y. Xuan, Spatio-temporal characteristics of the Portevin-Le Chatelier effect in austenitic steel with twinning induced plasticity, International Journal of Plasticity 25 (2009) 2298–2330.
[43] Z. Jiang, Q. Zhang, H. Jiang, Z. Chen, X. Wu, Spatial characteristics of the Portevin-Le Chatelier deformation bands in Al-4 at%Cu polycrystals, Materials Science and Engineering A 403 (2005) 154–164.
[44] Q. Lai, L. Brassart, O. Bouaziz, M. Gouné, M. Verdier, G. Parry, A. Perlade, Y. Bréchet, T. Pardoen, Influence of martensite volume fraction and hardness on the plastic behavior of dual-phase steels: experiments and micromechanical modeling, International Journal of Plasticity (2015).
[45] W. G. Johnston, J. J. Gilman, Dislocation velocities, dislocation densities, and plastic flow in lithium fluoride crystals, Journal of Applied Physics 30 (1959) 129–144.
[46] S. Venkadesan, P. Rodriguez, K. A. Padmanabhan, P. V. Sivaprasad, C. Phaniraj, Flow transients during strain rate jump tests in a titanium-modified austenitic stainless steel, Materials Science and Engineering A 154 (1992) 69–74.
[47] M. Isakov, S. Hiermaier, V. T. Kuokkala, Effect of Strain Rate on the Martensitic Transformation During Plastic Deformation of an Austenitic Stainless Steel, Metallurgical and Materials Transactions A: Physical Metallurgy and Materials Science 46 (2015) 2352–2355.
[48] T. Narutani, G. Olson, M. Cohen, Relations for austenitic steels during strain- induced martensitic transformation, Journal de Physique 43 (1982) 429–434.